The Astrophysical Journal, 660: L69–L72, 2007 May 1

AEGIS: INFRARED SPECTROSCOPY OF AN INFRARED-LUMINOUS LYMAN BREAK GALAXY AT $z = 3.01$

J.-S. Huang,[1] D. Rigopoulou,[2] C. Papovich,[3,4] M. L. N. Ashby,[1] S. P. Willner,[1] R. Ivison,[5] E. S. Laird,[6] T. Webb,[7] G. Wilson,[8] P. Barmby,[1] S. Chapman,[9] C. Conselice,[10] B. McLeod,[1] C. G. Shu,[11,12] H. A. Smith,[1] E. Le Floc'h,[3] E. Egami,[3] C. A. N. Willmer,[3] and G. G. Fazio[1]

Received 2006 May 31; accepted 2006 August 22; published 2006 September 20

ABSTRACT

We report the detection of rest-frame 6.2 and 7.7 μm emission features arising from polycyclic aromatic hydrocarbons (PAHs) in the *Spitzer* IRS spectrum of an infrared-luminous Lyman break galaxy at $z = 3.01$. This is currently the highest redshift galaxy where these PAH emission features have been detected. The total IR luminosity inferred from the MIPS 24 μm and radio flux density is $2 \times 10^{13}\ L_{\odot}$, which qualifies this object as a so-called hyperluminous infrared galaxy (HyLIRG). However, unlike local HyLIRGs, which are generally associated with QSO/AGNs and have weak or absent PAH emission features, this HyLIRG has very strong 6.2 and 7.7 μm PAH emission. We argue that intense star formation dominates the IR emission of this source, although we cannot rule out the presence of a deeply obscured AGN. This LBG appears to be a distorted system in the *HST* ACS F606W and F814W images, possibly indicating that a significant merger or interaction is driving the large IR luminosity.

Subject headings: cosmology: observations — galaxies: high-redshift — galaxies: starburst — infrared: galaxies

1. INTRODUCTION

Intensive star formation is a very common phenomenon in galaxies at high redshifts. Most high-redshift galaxies are detected because of their high star formation rates, revealed by either the rest-frame UV luminosity in Lyman break galaxies (LBGs; Steidel et al. 2003) or at far-infrared wavelengths in, for example, submillimeter-selected galaxies (SMGs; Chapman et al. 2003). It was long debated if LBGs and SMGs constituted different coeval populations. Recently, Chapman et al. (2005) found that some SMGs have similar $u - g$ and $g - R$ colors as LBGs. The *Spitzer Space Telescope* permits exploration of the rest-frame IR properties of LBGs. For example, Reddy et al. (2006) studied the 24 μm properties of $1.5 < z < 2.5$ LBGs and considered their relation to other galaxies at that epoch, including SMGs. Huang et al. (2005) reported that 5% of the LBGs at $z \sim 3$ in the sample of Steidel et al. (2003) are detected at 24 μm, and they defined this subpopulation as infrared-luminous Lyman break galaxies (ILLBGs). ILLBGs have IR properties very similar to submillimeter-selected sources (Egami et al. 2004; Huang et al. 2005; Pope et al. 2006). Huang et al. used *Spitzer* [3.6] − [8.0] and [8.0] − [24] colors to argue that the 24 μm emission from the majority of ILLBGs is powered by intensive star formation.

Observation of high-redshift galaxies with the Infrared Spectrograph (IRS; Houck et al. 2004) on board *Spitzer* permits the study of their 24 μm emission mechanism. Early IRS studies (Houck et al. 2005; Yan et al. 2005) have focused on 24 μm luminous ($f_{24} > 1$ mJy) and optically faint sources. Most of the objects in both samples of Houck et al. (2005) and Yan et al. (2005) are identified as dusty active galactic nuclei (AGNs) at $1.5 < z < 2.5$ whose spectra show power-law continua and strong silicate absorption but weak or absent emission features arising from the polycyclic aromatic hydrocarbon (PAH) molecules. Lutz et al. (2005) observed two lensed SCUBA sources at $z \sim 2.8$ with the IRS. Both sources are so-called hyperluminous IR galaxies (HyLIRGs; $L_{8-1000\,\mu\mathrm{m}} > 10^{13}\ L_{\odot}$) with strong PAH features.

For galaxies at $z > 2$, the Multiband Imaging Photometer for *Spitzer* (MIPS) 24 μm band detects rest-frame mid-IR continuum emission. At $z = 2.1$ and $z = 2.8$, the 6.2 and 7.7 μm PAH emission features respectively enter into the 24 μm band. Thus, a high-redshift, 24 μm–selected sample may preferentially select objects with strong emission-line features in the mid-IR bands. We have been studying just such a sample of LBGs, which have a redshift distribution centered at $\langle z \rangle = 3.0$ (Steidel et al. 2003).

This Letter presents the IRS spectrum and multiwavelength properties of one ILLBG at $z = 3.01$ detected in the Extended Groth Strip (EGS) area. The multiwavelength data set from the All-Wavelength Extended Groth Strip International Survey (AEGIS; Davis et al. 2007) including Advanced Camera for Surveys (ACS) images permits the study of spectral energy distribution (SED) and morphology of this source. We adopt $\Omega_m = 0.3$, $\Omega_\Lambda = 0.7$, and $H_0 = 70$ km s^{-1} Mpc^{-1}.

2. MULTIWAVELENGTH PHOTOMETRY AND INFRARED SPECTROSCOPY OF AN ILLBG

Most ILLBGs in the Huang et al. (2005) sample have 24 μm flux densities of ~0.1 mJy, too faint to permit efficient IRS

[1] Harvard-Smithsonian Center for Astrophysics, 60 Garden Street, Cambridge, MA 02138.
[2] Department of Astrophysics, Oxford University, Keble Road, Oxford OX1 3RH, UK.
[3] Steward Observatory, University of Arizona, 933 North Cherry Avenue, Tucson, AZ 85721.
[4] Spitzer Fellow.
[5] Royal Observatories Edinburgh, Blackford Hill, Edinburgh EH9 3HJ, UK.
[6] UCO/Lick Observatory, University of California, Santa Cruz, CA 95064.
[7] Department of Physics, McGill University, 3600 rue University Montréal, QC H3A 2T8, Canada.
[8] *Spitzer* Science Center, California Institute of Technology, Mail Code 314-6, 1200 East California Boulevard, Pasadena, CA 91125.
[9] Department of Astronomy, California Institute of Technology, Pasadena, CA 91125.
[10] Department of Astronomy, Nottingham University, University Park, Nottingham NG7 2RD, UK.
[11] Joint Astrophysics Center, Shanghai Normal University, Shanghai 200234, China.
[12] Shanghai Astronomical Observatory, Chinese Academy of Sciences, 80 Nandan Lu, Shanghai 2000030, China.

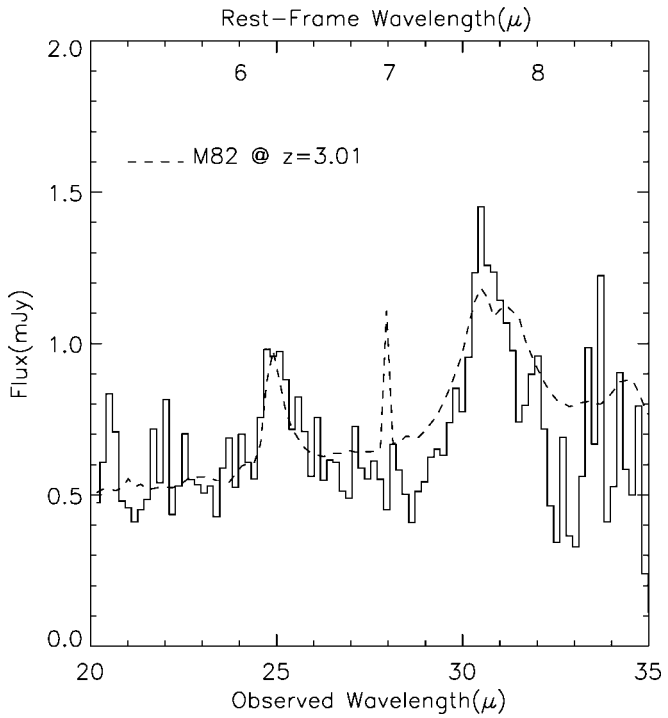

FIG. 1.—IRS spectrum of EGS20 J1418+5236. The dashed line is the M82 SED shifted to $z = 3.01$.The spectrum has remarkably similar 6.2 and 7.7 μm PAH emission-feature strength and shape to those of M82. We cross-correlated the IRS spectrum with that of M82 to derive a redshift of $z = 3.01 \pm 0.016$. The IRS spectrum at $\lambda > 32$ μm becomes very noisy, so the 8.2 μm PAH emission feature is not detected.

observations.[13] M. Ashby et al. (2007, in preparation) performed a wide-field deep u' and g' imaging survey with the Megacam on the MMT, covering the whole EGS and overlapping with deep Subaru *R*-band imaging and *Spitzer* MIPS data. The goal of the MMT Megacam survey is to obtain an ILLBG sample with higher 24 μm flux density for IRS spectroscopic followup. J.-S. Huang et al. (2007, in preparation) give a detailed description of this sample. Objects with strong AGN activity, such as QSOs, are excluded from the sample using combinations of [3.6] − [8.0] and [8.0] − [24] colors (Ivison et al. 2004; Huang et al. 2005). Spectroscopic redshifts for this sample are not yet available. We selected the object that is the subject of this Letter, EGS20 J1418+5236 (hereafter E21, the 21st in the IRS target list), as a LBG with $u' - g' > 1.4$, $g' - R = 0.39$, and $R = 24.30$, and with very strong 24 μm emission, $f_{24} = 0.62$ mJy.

We obtained a spectrum for E21 with the IRS using the Long-Low module (LL1) in staring mode, covering 20–39 μm (see Fig. 1). We observed the source for 24 cycles of 120 s duration. The total on-source integration time was 5851 s. We combined the reduced frames, subtracted residual background counts, and used the SMART package (Higdon et al. 2004) to extract calibrated one-dimensional spectra for both positive and negative beams. The final IRS spectrum is an average of both beams. The spectrum shows a significant detection of 6.2 and 7.7 μm PAH emission features at $z = 3.01 \pm 0.016$. This is consistent with a typical redshift for *u*-dropout–selected LBGs. Given the presence of multiple emission features in the IRS spectrum here, the redshift accuracy is significantly better than that reported for other $z > 2$ sources in the literature. Spectra of other objects often have a low signal-to-noise ratio, only a single emission feature, or a featureless spectrum (e.g., Houck et al. 2005; Yan et al. 2005).

The AEGIS multiwavelength data set permits the study of E14 from X-rays to the 20 cm radio band. While there is a single source in the MMT u', g', and Subaru *R* images, the *Hubble Space Telescope* ACS images resolve this galaxy into two components, which we refer to as J1 and J2 (Fig. 2). In addition, another object, called J3, resides 3″ to the east of J1 and J2 and could contaminate the *Spitzer* IR emission. Strong emission at u' from J3 suggests that it is at a much lower redshift, and using the full data set we derive a photometric redshift of $z = 0.79$. J3 is not detected at 20 cm (5 σ limit of

[13] See http://ssc.spitzer.caltech.edu/irs/documents/irs_ultradeep_memo.pdf.

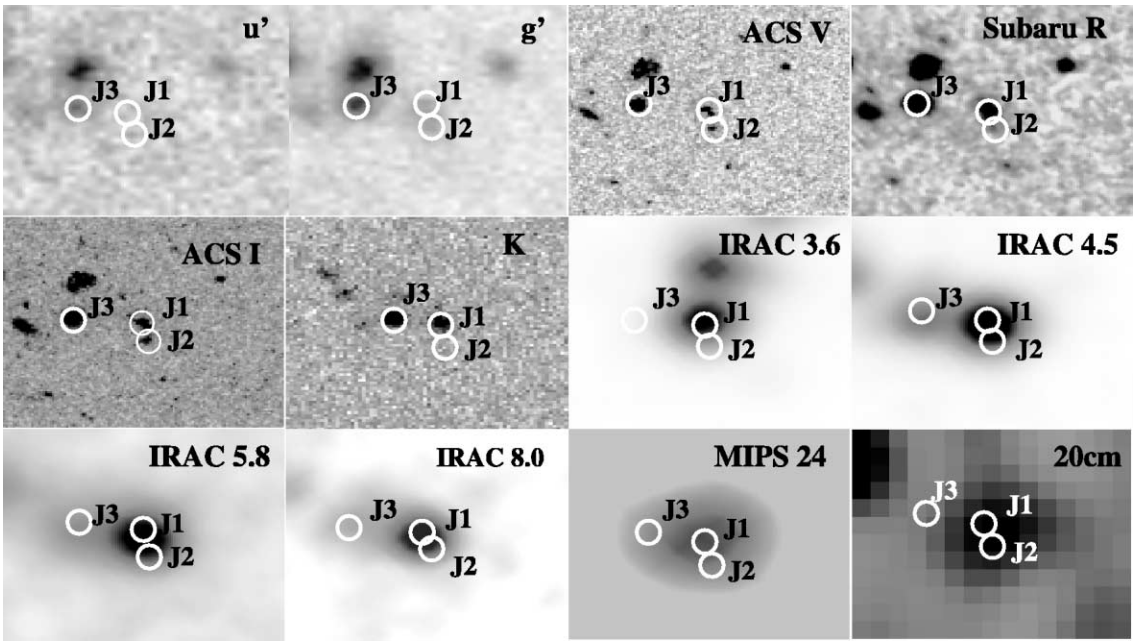

FIG. 2.—Multiwavelength stamp images for EGS20 J1418+5236. The spatial resolutions are 1″ for the MMT Megacam u' and g' images, 0.″6 for the Subaru *R*-band image, 0.″1 for the ACS *V*- and *I*-band images, 0.″8 for the Palomar *K*-band image, 1.″8–2.″2 for the four IRAC bands, 5″ for the MIPS 24 μm band, and 3″ for the VLA 20 cm image.

$f_{20\,\mathrm{cm}} < 42$ μJy, compared to the 10 σ detection of the J1+J2 component with $f_{20\,\mathrm{cm}} = 82$ μJy; Ivison et al. 2007). Therefore, we conclude that the J3 component does not contribute to the 24 μm flux density or the emission in the IRS spectrum.

Both J1 and J2 are so-called u' dropouts (e.g., Steidel et al. 2003) and show low surface brightness features that connect to J1 and J2 in the ACS *V*- and *I*-band images. The two components are separated by 0.″8, or 6.24 kpc, at $z = 3.01$. These facts suggest that J1 and J2 belong to an interacting/merging system. The two components have different colors: J1 is red ($V_{\mathrm{AB}} - I_{\mathrm{AB}} = 0.97$), and J2 is blue ($V_{\mathrm{AB}} - I_{\mathrm{AB}} = 0.65$). J1 is detected in both the *J* and K' bands, but J2 is not detected to $K_{\mathrm{limit,\,AB}} = 22.4$. J1 has $J_{\mathrm{AB}} - K_{\mathrm{AB}} = 0.88$ (or 1.9 in the Vega system). We argue that J1 is mainly responsible for the Infrared Array Camera (IRAC), MIPS 24 μm, and radio flux densities and for the emission in the IRS spectrum. With $K_{\mathrm{AB}} = 20.89$ for J1 and $K_{\mathrm{limit,\,AB}} = 22.4$ for J2, J2 may contribute less than 11% of the IR emission of this system (see Fig. 3).

3. INFRARED PROPERTIES OF E21

Both the continuum and the 6.2 μm PAH emission feature contribute to the 24 μm flux density ($f_{24} = 0.62$ mJy) of E21. We measure the continuum emission as 0.55 mJy in the observed wavelength range of 20 $\mu\mathrm{m} < \lambda < 32.5$ μm; thus, the contribution of the 6.2 μm PAH emission to the MIPS 24 μm flux density is 0.07 mJy. Most ILLBGs have 24 μm flux densities of ~0.06–0.1 mJy (Huang et al. 2005). If other ILLBGs have comparable emission-line fluxes, then this line would contribute significantly to their 24 μm flux densities.

The power mechanism for the mid-IR emission of ILLBGs remains unclear. PAH emission features are associated with intensive star formation (Rigopoulou et al. 1999; Lu et al. 2003; Lutz et al. 2005). Rigopoulou et al. (1999) suggest that the 7.7 μm feature-to-continuum ratio, L/C, can be used to classify AGNs and starburst galaxies in ultraluminous infrared galaxy (ULIRG) samples: $L/C > 1$ for starburst galaxies and $L/C < 1$ for AGNs. Although a few AGN-dominated ULIRGs and most type II AGNs could have $L/C > 1$ (Lu et al. 2003), a large 7.7 μm L/C value does at least suggest that intensive star formation is the dominant energy source. Peeters et al. (2004) argued that the 6.2 μm PAH emission feature is a better indicator to separate starbursts and AGNs: QSO and type I AGNs have typical feature-to-continuum ratios of 0.1, and starburst ULIRGs and type II AGNs have a lower value in range of $0.5 < L/C < 2$. The 6.2 and 7.7 μm feature-to-continuum ratios for E21 are 0.40 and 1.8, respectively, consistent with values of starburst ULIRGs. Furthermore, the limit on X-ray emission from E21 in the 200 ks *Chandra* observation (P. Nandra et al. 2007, in preparation) is $L_{2-10\,\mathrm{keV}} < 1.0 \times 10^{43}$ ergs s^{-1}, suggesting the absence of strong AGN activity. Two other high-redshift SMGs with IRS spectroscopy are identified as AGN-dominated ULIRGs with similar IR luminosities *and* strong X-ray emission: SMM J02399−0136 at $z = 2.8$ (Lutz et al. 2005), which, much like this source, has rather strong PAH emission; and CXO J141741.9+582823 at $z = 1.15$ (Le Floc'h et al. 2007), which has no PAH emission features. Furthermore, even when AGNs are detected in high-redshift SMGs based on their X-ray emission, Alexander et al. (2005) argue that substantial ongoing star formation dominates the IR emission in these objects. Thus, we argue that intensive star formation is the dominant energy source for the IR emission of E21. The different types of IR-luminous, high-redshift sources may represent different stages of HyLIRGs: starburst-dominated E21 with strong PAH and no X-ray emission; intermediate-type SMM J02399−0136 and other SMGs with both PAH and detected X-ray emission; AGN-dominated CXO J141741.9+582823 with no PAH but strong X-ray emission.

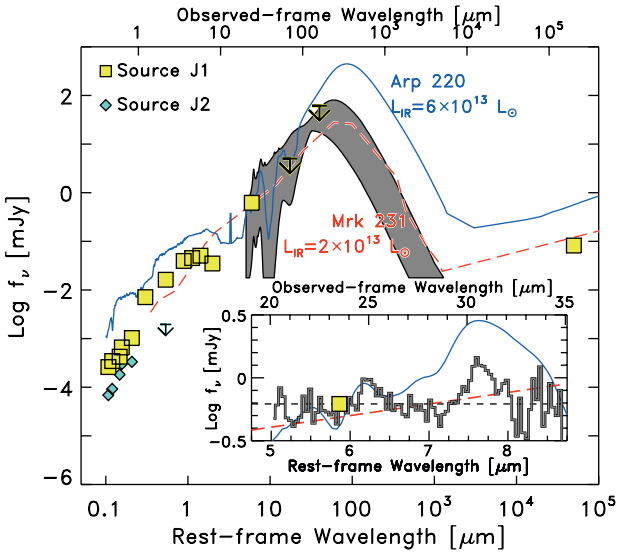

FIG. 3.—SEDs for both J1 and J2. The yellow boxes show the SED for J1, and cyan diamonds show the SED for J2. Upper limits on the flux density (5 σ) are denoted by downward arrows. The blue solid line shows the SED for Arp 220 (Chary & Elbaz 2000), and the red dashed line shows the SED of Mrk 231, in both cases normalized to the flux density at 24 μm. J2 is not detected in either the *J*- or *K*-band images. Because J2 should not be redder than J1, we use the J1 and J2 *K*-band flux ratio (with the limiting flux for J2) to estimate that J2 should contribute less than 11% to the IRAC and MIPS 24 μm photometry. We use both the Arp 220 and Mrk 231 SED models to estimate the total IR luminosity of this source using the 24 μm flux density. The Mrk 231 SED model with $L_{8-1000\,\mu\mathrm{m}} = 2 \times 10^{13}$ is in better agreement with the far-IR and radio flux densities. Similarly, the gray-shaded region shows the range of theoretical SEDs of Siebenmorgen & Krügel (2007) for starburst-powered IR-luminous galaxy models with $L_{8-1000\,\mu\mathrm{m}}$ consistent with that estimated from the radio emission. Note that these models have not been rescaled to fit the observed photometry, but instead we show the predicted flux densities for a galaxy at $z = 3.01$. The inset plot shows the IRS spectrum. The horizontal dashed line shows the observed 24 μm flux density (*yellow box*), and the other curves are the SEDs of Arp 220 and Mrk 231 as for the main figure.

Currently, there is no submillimeter observation of this source. We use the 20 cm radio flux and $f_{850\,\mu\mathrm{m}}/f_{20\,\mathrm{cm}}$ redshift relation (Carilli & Yun 2000; Dunne et al. 2000; Wang et al. 2004a) to predict that E21 has an 850 μm flux density of 10 mJy $< f_{850\,\mu\mathrm{m}} <$ 17 mJy. Similarly, we derive the rest-frame far-IR luminosity using the far-IR–radio luminosity relation (Condon 1992; Carilli & Yun 2000):

$$L_{\mathrm{FIR}} = 4\pi D_l^2 f_{20\,\mathrm{cm}} 10^q (1+z)^{-(1+\alpha)}, \quad (1)$$

$$L_{8-1000\,\mu\mathrm{m}} = 1.92 L_{\mathrm{FIR}}, \quad (2)$$

where $q = \log(f_{\mathrm{FIR}}/f_{20\,\mathrm{cm}}) = 2.34$, and the radio spectral index $\alpha = -0.8$. For $f_{20\,\mathrm{cm}} = 0.082$ mJy at $z = 3.01$, $L_{8-1000\,\mu\mathrm{m}}$ is equal to $2 \times 10^{13}\,L_\odot$, qualifying this source as a HyLIRG.

Fitting the SED with various galaxy templates yields a similar IR luminosity. We normalize the SEDs of two local ULIRGs, Arp 220 and Mrk 231, to the 24 μm flux density to predict the total IR luminosity for this source: 6×10^{13} and $2 \times 10^{13}\,L_\odot$, respectively. (Fig. 3). The Arp 220 SED model predicts a much higher far-IR and radio flux density than ob-

served. The Mrk 231 SED provides a consistent interpretation to both the 24 μm and radio flux densities as well as the 70 and 160 μm flux limits. Similarly, Figure 3 also compares the observed SED to models with IR luminosity $L_{8-1000\,\mu\mathrm{m}} = 10^{13.2}$–$10^{13.3}\,L_{\odot}$ (i.e., consistent with that derived from the radio emission) from Siebenmorgen & Krügel (2007). The models broadly agree with the 24 μm flux density (and the limits at 70 and 160 μm) and provide further evidence that the SED is dominated by emission from hot dust. This is also consistent with strong continuum emission in the IRS spectrum. Therefore, given the constraints from the empirical and theoretical models, we conclude that hot dust dominates the far-IR emission in this object.

This source is very unlikely to be amplified due to gravitational lensing. Gravitational lensing is very inefficient for J3 being a lensing galaxy at $z = 0.79$. There are also no clusters or groups found in the area. Furthermore, the galaxy morphologies in the ACS image and color difference of J1 and J2 do not support strong lensing for this source.

The morphology of E21 is reminiscent of those of local ULIRGs. Locally, about one-third of ULIRGs have double nuclei with a mean linear separation of 6.2 kpc (e.g., Rigopoulou et al. 1999; Surace & Sanders 2000). E21 appears to have multiple components in the ACS images (see Fig. 2). The projected separation of J1 and J2 is 6.75 kpc. UV luminosity is a direct measurement for the relatively unobscured massive star formation in ULIRGs. Although ULIRGs are dusty, they typically have strong UV emission (e.g., Surace & Sanders 2000), although this emission often stems from separate star-forming regions rather than those that dominate the IR (and bolometric) emission (e.g., Zhang et al. 2001; Wang et al. 2004b). The U ($\lambda_{\mathrm{central}} = 3414$ Å) luminosities, νL_{ν}, for ULIRGs (Surace & Sanders 2000) cover a large range, from 10^{9} to $5 \times 10^{11}\,L_{\odot}$, with an average of $2 \times 10^{10}\,L_{\odot}$. At $z \sim 3$, the observed J band probes roughly the rest-frame U band. We use the J-band magnitude to estimate the rest-frame U luminosity for EGS20 J1418+5236, $\nu L_{\nu}(U) = 3.5 \times 10^{11}$, roughly 1%–2% of the bolometric emission. This is consistent with its local IR-luminous galaxy counterparts.

4. CONCLUSIONS

IRS spectra of EGS20 J1418+5236, a $z = 3.01$, u-dropout LBG in AEGIS show the 6.2 and 7.7 μm PAH emission features. This is currently the highest redshift galaxy where the PAH emission features have been detected. This source has a total infrared luminosity of $L_{8-1000\,\mu\mathrm{m}} = 2 \times 10^{13}\,L_{\odot}$ inferred from both the 24 μm and radio flux densities. Nearby galaxies with these IR luminosities are predominantly QSOs/AGNs, but given the presence of strong PAH emission features and the lack of any evidence for an AGN, we conclude that star formation dominates the emission from this $z = 3$ ILLBG.

The 24 μm–to–radio flux ratio, strong IRS continuum emission, and upper limits on the flux density at 70 and 160 μm implies that hot dust dominates the far-IR emission in this object, very similar to Mrk 231 and model SEDs of HyLIRGs. Interestingly, the theoretical models that best describe the shape and relative strength of the mid-IR SED require very high extinction values ($A_V \gtrsim 70$ mag). Because this object has strong UV emission, we suggest that this LBG contains a deeply embedded starburst in addition to the relatively unobscured stars that dominate the rest-frame UV optical emission. This scenario may explain the general UV-IR properties of the ILLBG population. This example suggests that HyLIRGs at high redshifts can appear as either ILLBGs, or SMGs, or both. Larger samples of $z \sim 3$ galaxies with IRS spectroscopy and measurements of their far-IR SEDs are clearly needed to confirm these hypotheses.

We wish to thank our collaborators on the AEGIS project for many insightful conversations and much hard work. This work is based in part on observations made with the *Spitzer Space Telescope*, which is operated by the Jet Propulsion Laboratory, California Institute of Technology, under a contract with NASA. Support for this work was provided by NASA through an award issued by JPL/Caltech.

REFERENCES

Alexander, D. M., Bauer, F. E., Chapman, S. C., Smail, I., Blain, A. W., Brandt, W. N., & Ivison, R. J. 2005, ApJ, 632, 736
Carilli, C. L., & Yun, M. 2000, ApJ, 539, 1024
Chapman, S., Blain, A. W., Ivison, R. J., & Smail, I. R. 2003, Nature, 422, 695
Chapman, S., Blain, A. W., Smail, I., & Ivison, R. J. 2005, ApJ, 622, 772
Chary, R., & Elbaz, D. 2000, BAAS, 32, 1510
Condon, J. J. 1992, ARA&A, 30, 575
Davis, M., et al. 2007, ApJ, 660, L1
Dunne, L., Clements, D. L., & Eales, S. A. 2000, MNRAS, 319, 813
Egami, E., et al. 2004, ApJS, 154, 130
Higdon, S. J. U., et al. 2004, PASP, 116, 975
Houck, J., et al. 2004, ApJS, 154, 18
———. 2005, ApJ, 622, L105
Huang, J.-S., et al. 2005, ApJ, 634, 137
Ivison, R., et al. 2004, ApJS, 154, 124
———. 2007, ApJ, 660, L77
Le Floc'h, E., et al. 2007, ApJ, 660, L65
Lu, N., et al. 2003, ApJ, 588, 199
Lutz, D., et al. 2005, ApJ, 625, L83
Peeters, E., Spoon, H. W. W., & Tielens, A. G. G. M. 2004, ApJ, 613, 986
Pope, A., et al. 2006, MNRAS, 370, 1185
Reddy, N. A., Steidel, C. C., Fadda, D., Yan, L., Pettini, M., Shapley, A. E., Erb, D. K., & Adelberger, K. L. 2006, ApJ, 644, 792
Rigopoulou, D., Spoon, H. W. W., Genzel, R., Lutz, D., Moorwood, A. F. M., & Tran, Q. D. 1999, AJ, 118, 2625
Siebenmorgen, R., & Krügel, E. 2007, A&A, 461, 445
Steidel, C. C., Adelberger, K. L., Shapley, A. E., Pettini, M., Dickinson, M., & Giavalisco, M. 2003, ApJ, 592, 728
Surace, J., & Sanders, D. 2000, AJ, 120, 604
Wang, W.-H., Cowie, L. L., & Barger, A. J. 2004a, ApJ, 613, 655
Wang, Z., et al. 2004b, ApJS, 154, 193
Yan, L., et al. 2005, ApJ, 628, 604
Zhang, Q., Fall, S. M., & Whitmore, B. C. 2001, ApJ, 561, 727